

Heat transfer from tube banks to air/water mist flow

WATARU NAKAYAMA, HEIKICHI KUWAHARA and SHIGEKI HIRASAWA

Mechanical Engineering Research Laboratory, Hitachi, Ltd., 502 Kandatsu, Tsuchiura,
Ibaraki 300, Japan

(Received 31 August 1987)

Abstract—Heat transfer and pressure drop data were obtained with the banks of smooth tubes, microfinned tubes, and finned tubes placed in the mist stream, where the air velocity was in the range of $1\text{--}3\text{ m s}^{-1}$, and the water mass flux $50\text{--}390\text{ kg m}^{-2}\text{ h}^{-1}$. Cross examinations of the heat transfer data indicate that evaporation of water from the wetted part of the surface area is a primary mechanism of heat transfer enhancement. Based on the empirical correlations for the effective wet area on the heat transfer surface, the method of heat exchanger design is proposed. The pressure drop data show little difference between the flow resistance in mist flows and that in single phase air flows.

INTRODUCTION

IN MANY industrial applications the demand to conserve water resources has promoted the replacement of wet cooling towers with air-cooled heat exchangers. The air-cooled heat exchanger, however, is bulky, and consumes fan power which amounts to a large parasitic power expense of the host system. These drawbacks of the air-cooled heat exchanger can be compensated by the use of the dry/wet scheme, where during the period of high ambient temperature, the task of heat rejection is assisted by water spray directed to the core of the heat exchanger. The feasibility of the dry/wet scheme has been studied for geothermal power plants [1] and large-scale power plants to be located in arid regions [2]. There are many other potential applications in air-conditioning and refrigeration systems [3], cooling systems for electronic equipment, to cite only a few. The present work is concerned with the wet phase of the heat exchanger operation. The term 'mist cooled heat exchanger' will be used throughout this paper, for it helps to describe the physical situation studied here.

The success in the design of the dry/wet heat exchange system critically depends on the basic understanding of the performance of the mist cooled heat exchanger. An optimistic estimation of the wet phase performance could force the plant operation below its normal rating in the adverse climate, while a too conservative estimation negates the potential advantage to be gained on the dry/wet system. There are many factors involved in the design of the mist cooled heat exchanger; the fundamental ones among them are the structure of the heat exchanger core, the direction of air flow, and the direction of water injection. The present work deals with the heat exchanger core composed of horizontal tubes, arranged in a bank deep in the vertical direction and relatively short in the

direction of the air stream. The air is blown horizontally across the tube bank, and water mist is borne in the air stream.

Finlay and McMillan [4] obtained the data with the tube bank, and reported the significant effect of the water spray in heat transfer enhancement. Oshima *et al.* [5] proposed the formula for the design of mist cooled heat exchangers on the assumption that the tubes are fully wet. Tree *et al.* [6] conducted experiments with a fin and tube heat exchanger with relatively small rates of water supply, and reported that the performance of the heat exchanger is sensitive to the mass flux of water mist. They also reported the difficulty in extending the wet zone toward the rear part of the heat exchanger. Carpenter [7] pointed out the effect of the air velocity on the transport of water separated in droplets from a tube to another, thereby yielding an appreciable influence on the heat exchanger performance.

Besides the above works on the bank of horizontal circular tubes, there are reports on the cases of other heat exchanger geometries and different directions of air-water mixture [8-14].

Those previous works indicate the importance of wetting as wide a surface area of the heat exchanger as possible in achieving high levels of heat transfer enhancement. Some data in the literature show that the water spray on the heat exchangers of conventional design produces a certain effect, yet the effect is not impressive due to the stagnation of arrested water in the upstream region of the heat exchanger core [6, 10]. The structure of the heat exchanger core should be designed so as to effectively spread the wet zone toward the downstream end. Spread of the wet zone depends primarily on two factors; the dynamics concerning the arrest of water droplets by the heat exchanger surface, and the mechanism of spread of water film on the surface.

NOMENCLATURE

<p>A surface area of the tube [m²]</p> <p>A_c projected frontal area of the tube [m²]</p> <p>A_{ev} effective wet area [m²]</p> <p>c_p specific heat [J kg⁻¹ K⁻¹]</p> <p>d base diameter of the tube [m]</p> <p>h heat transfer coefficient [W m⁻² K⁻¹]</p> <p>h_{fg} latent heat of evaporation [J kg⁻¹]</p> <p>k thermal conductivity [W m⁻¹ K⁻¹]</p> <p>Δi enthalpy potential for evaporation [J kg⁻¹]</p> <p>\dot{M}_a mass flow rate of air [kg s⁻¹]</p> <p>M_d rate of water drainage from the tube [kg s⁻¹]</p> <p>\dot{M}_{ev} evaporation rate of water [kg s⁻¹]</p> <p>\dot{m} water mass flux [kg m⁻² s⁻¹]</p> <p>\dot{m}_i specific water supply rate defined in regard to the frontal area of the tube [kg m⁻² s⁻¹ or kg m⁻² h⁻¹]</p> <p>Nu Nusselt number, equation (2)</p> <p>p_t tube pitch [mm]</p> <p>Q heat transfer rate [W]</p> <p>Q_L rate of latent heat transport by evaporation of water [W]</p> <p>Q_s enthalpy input from arrested water droplets [W]</p>	<p>q heat flux [W m⁻²]</p> <p>Re Reynolds number, equation (3)</p> <p>T_a dry-bulb temperature [°C]</p> <p>T_{as} wet-bulb temperature [°C]</p> <p>T_w tube wall temperature [°C]</p> <p>ΔT temperature difference [K]</p> <p>V_a frontal air velocity [m s⁻¹]</p> <p>V_{\min} air velocity at the minimum free flow area [m s⁻¹]</p> <p>x absolute humidity in the air stream [kg kg⁻¹]</p> <p>x_1 absolute humidity of saturated air at T_w [kg kg⁻¹].</p> <p>Greek symbols</p> <p>ν kinematic viscosity of air [m² s⁻¹]</p> <p>ϕ coefficient in equation (5).</p> <p>Suffixes</p> <p>a air</p> <p>c convective heat transfer</p> <p>i index of vertical row</p> <p>j index of horizontal row</p> <p>l water.</p>
---	--

To promote the latter, the authors provided the tube's surface with microfins and porous structures, and investigated the effect of those microstructures by placing a test tube in the stream of the air–water mixture [15]. This paper reports the data obtained with the bank of tubes. Three types of tubes were used to form the banks; smooth tube, microfinned tube, and finned tube. The microfinned tube has fins of a particular shape, 1 mm high and spaced with a pitch of 0.7 mm. The previous investigation [15] proved that the microfins are effective in expanding the area for water evaporation. The finned tube has fins 5 mm in height and spaced with a pitch of 2.5 mm. Crisscrossing minute grooves are provided on the aluminum fin surface by the knurling tool in an attempt to aid spread of water film over the surface. The test tubes are arranged in a triangular pattern with a pitch of either 54 or 42 mm. The heat transfer data were sampled at selected locations in the tube bank. Those data revealed the spatial variation of the heat transfer coefficient in the bank, a novel contribution to the existing body of knowledge about mist cooled heat exchangers. There is another aspect of the present investigation to be contrasted to the other investigations. The experimental investigation was focused on the case of a relatively low air stream velocity, that is 1–3 m s⁻¹, considering the demand on reduced air velocities in many industrial applications. The cost optimization for the binary cycle power plant

on geothermal energy [16] shows that the optimum air velocity actually exists in the low velocity range. The consequence of the low velocity air stream is the mode of water drainage within the tube bundle, where the drainage tends to travel vertically from upper to lower tubes, thereby affecting heat transfer on the tubes at lower levels.

EXPERIMENTAL APPARATUS AND TEST TUBES

Figure 1(a) shows the schematic diagram of the experimental apparatus. The wind tunnel having a square cross section of 50 × 50 cm is set horizontally. From the inlet downstream are installed the vanes to control the flow rate of air (⑤), the blower (③), the rectifier grid (④), the water spray nozzles (⑥), the hot wire anemometer or the mist sampling probe (⑧), the test tube bank (②), and the vanes to arrest water droplets from the exhaust stream (①). The distance between the location of the water spray and the first row of tube banks is 1500 mm, and the velocity measurement and the mist sampling are conducted 150 mm upstream of the tube bank. The section of the duct wall between the spray nozzle assembly and the eliminator vanes (⑨) is made transparent by using the acrylic plates to enable the visualization of mist flows and the process of water arrest and drainage in the tube bank.

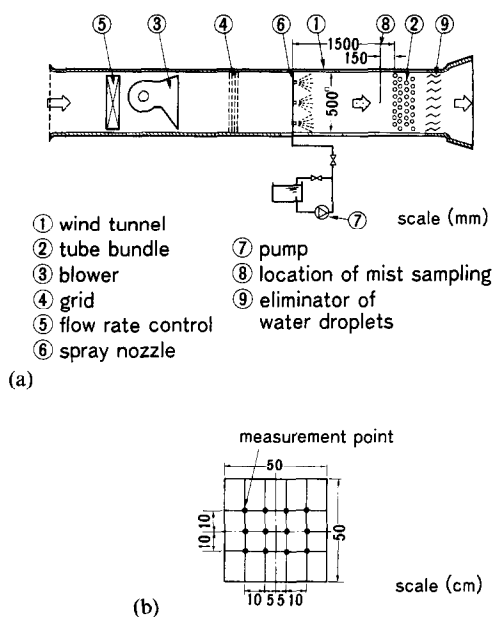


FIG. 1. Experimental apparatus: (a) overall set-up; (b) points of mist sampling.

At the location of the water spray nine nozzles are installed in a 3×3 square net pattern. The water pressure at the back of the nozzle is regulated at the level of 7.8×10^5 Pa. The change of spray rate is effected by replacing all the nozzles with those of a different rating. The nozzles of three different spray ratings, 0.48, 1.05, and $2.37 \text{ cm}^3 \text{ s}^{-1}$, all manufactured by DeLaval Co., were used in this experiment. The mist sampling probe has the same structure as the one reported in ref. [15]. The tubular probe has a 19 mm i.d. and a 25 mm long intake section extending toward the oncoming flow. Water caught in the intake is brought down the vertical stem by the combined action of gravity and the capillarity of the cloth liner provided in the probe, then collected in the beaker at the bottom. The mass flux of water is determined from the weight of water collected per unit time and the cross-sectional area of the probe. Air is allowed to flow in the probe, then toward the laboratory from the bottom of the vertical stem. At this end of the air exhaust the dry-bulb temperature and the wet-bulb temperature are measured by the thermocouples. The thermocouple for the wet-bulb temperature measurement is covered by a cotton gauze which extends down to the collected water in the beaker. The probe was traversed in the cross-section of the duct, and the sampling was made at 12 spots shown in Fig. 1(b). It was found that the distribution of mist flux reflects the effect of gravity on the trajectory of water droplets from the nozzle to the point of measurement. Namely, the mass flux at the top level of the measurement grid is lower than that at the middle and bottom levels, the maximum difference reaching almost 30% of the flux at the lower levels. There is also a variation of a comparable magnitude in the mass flux distribution

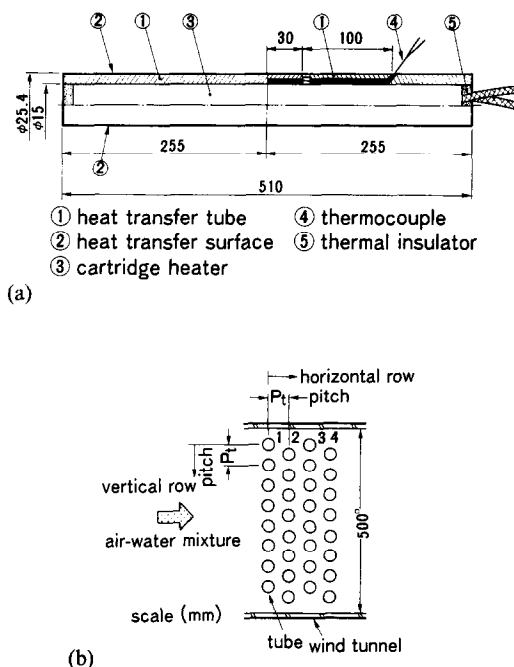


FIG. 2. Test tube: (a) longitudinal cross-section of the test tube; (b) cross-section of tube bank.

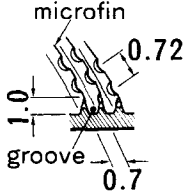
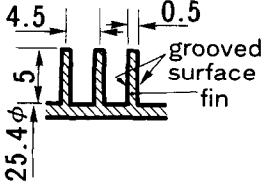
along the horizontal axes. However, at the points on the central two columns of the grid, the variation of mass flux was within $\pm 13\%$ of the average value of the fluxes at those points. The heat transfer measurements were made at the middle sections of the tubes, hence, it may be assumed that they produced the data in the condition of nearly uniform mist flow distribution at the front of the tube bank. In reporting the data the average value of the mass fluxes at the central two points on the middle horizontal axis is used.

The distribution of air velocity was measured at the mist sampling location (Fig. 1(a) ⊙). The hot-wire anemometer was traversed in the cross-section before the start of the wet run. It was found that the variation of air velocity in the cross-section was within 10% when the average velocity was 1 m s^{-1} and 2% at 5 m s^{-1} . In reporting the data the velocity measured at the middle point is used.

The static pressure on the duct wall was measured at the two spots on the duct ceiling, 150 mm upstream of the front of the tube bank and 150 mm downstream from the back of the bank.

Figure 2(a) shows the longitudinal cross-section of the test tube. The tube is made from corrosion resistant aluminum or pure aluminum. It extends across the width of the duct, with the margins at the ends to be fit in the holes on the duct wall. The diameter of the tube, prior to the machining in the case of the microfinned tube and the fin bonding in the case of the finned tube, is 25.4 mm. The tube is equipped with the cartridge heater inside, and four thermocouples in its 5 mm thick wall. The thermocouple is formed by

Table 1. Tested tube banks (scale, mm)

Test tube	Smooth tube	Microfinned tube	Finned tube
surface	smooth		
outside diameter	25.4	25.4 (prior to machining)	25.4 (base diameter)
material		corrosion resistant aluminum	aluminum
pitch	54	54	42
vertical row	4	4	4
horizontal row	8	8	11

copper and constantan wires, each 0.2 mm in diameter, and located at the middle of the tube length. Its leads run through the 130 mm long hole provided in the wall before leaving the tube. Such arrangements are provided on the four locations along the circumference of the tube at an interval of 90°. The wall temperature reported in this paper is the average of the readings of those four thermocouples. Due to the relatively thick tube wall and large thermal conductivity of aluminum only a small variation of temperature, 2–3 K in most experimental runs, was found.

Figure 2(b) shows the cross-section of the tube bank. There are four vertical rows, and eight or eleven horizontal rows depending on whether the pitch of tube arrangement is 54 or 42 mm. The power input to the tube's heater was controlled individually, so that the distribution of tube temperature in the bank was made nearly uniform, to within ± 1.5 K. In this experiment measurements of heat transfer coefficient were made for the sample tubes in the bank; where the tube pitch (p_i) is 54 mm, the sample tubes are on the third, fifth, and sixth horizontal rows, and where $p_i = 42$ mm, on the fourth, sixth, and eighth rows. The rate of power supply is divided by the surface area of the cylinder 25.4 mm in diameter and 500 mm in length to obtain the nominal heat flux (q).

The heat transfer coefficient (h) is defined by

$$h = \frac{q}{\Delta T} \quad (1)$$

where ΔT is the difference between the tube wall temperature (T_w) and the dry-bulb temperature (T_a) of the air in front of the tube bank. Heat loss to the duct wall through the ends of the tube is estimated to be negligibly small.

Table 1 shows the specifications of the test tube banks. The smooth tube and the microfinned tube are made from corrosion resistant aluminum (A 5052). To erect microfins the 25.4 mm diameter tube is first given rows of minute grooves on its outer surface by the knurling process, then the spiral fin is scraped up by the tool head on the lathe. This machining pro-

duces the fins of a saw-tooth shape; the fin height is 1 mm and the fin pitch is 0.7 mm. This process was originally developed for the enhanced condenser tube [17], and the microfinned surface was proved by the previous investigation [15] to be effective in spreading the water film over the tube surface by capillary action. With the bank of microfinned tubes the effect of tube placement pitch was investigated. The finned tube was made by winding an aluminum strip on a 25.4 mm diameter aluminum tube. The fin base was then firmly bonded by soldering. The height of the fin is 5 mm, the thickness 0.5 mm, and the pitch 4.5 mm. On the surface of the fin crisscrossing minute grooves were provided by the knurling tool. The grooves, 0.2 mm deep and spaced at 0.7 mm, are expected to help spread the water film over the fin surface.

The experiments were performed in the following parametric range:

air velocity in front of the tube bank	1, 2, 3 m s ⁻¹
dry-bulb temperature of air at the bank front	11–21°C
mass flux of water	50–390 kg m ⁻² h ⁻¹
water temperature at the base of the nozzle	13–25°C
average water droplet diameter	40 μm
standard deviation of droplet diameter	14 μm
relative humidity in front of the tube bank	84–95%
tube wall temperature	20–80°C.

The diameters of water droplets were measured by arresting droplets on a glass plate coated with silicone oil film [15]. The laboratory tap water was led to the nozzles without modulation of its temperature. In each experimental run, however, the temperature difference between the incoming air and the water at the supply reservoir was relatively small, less than 3 K with tap water being warmer than air in most of the runs. The heat exchange between air and water

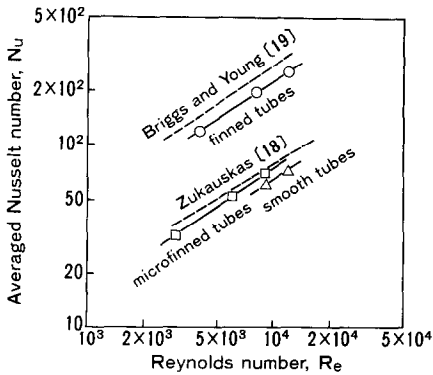


FIG. 3. Averaged Nusselt number for the tube bank in single phase flow of air.

droplets during the flight of droplets in the 1.5 m length might reduce the temperature difference further and bring the droplet temperature close to the wet-bulb temperature which was measured at the base of the mist sampling probe as noted previously.

The estimations of accuracies in the measurements of mist flux, droplet temperature, wet-bulb temperature, and heat transfer coefficient are themselves challenging due to the uncertainties in physical processes affecting the measurements. The accuracy analysis, therefore, is not developed here; instead, the resolution limits of the instruments are noted as follows: the thermometry 0.1 K, the hot-wire anemometer 0.05 m s^{-1} , the weight scale for mist flux measurement 0.01 g, the wattmeter for the measurement of power input to the heater 0.1 W.

RESULTS OF HEAT TRANSFER EXPERIMENTS

Single-phase flow heat transfer

The data obtained in the absence of water mist are reduced to the Nusselt number

$$Nu = \frac{h_c d}{k_a} \quad (2)$$

where d is the base diameter of the tube (25.4 mm), and k_a is the thermal conductivity of air at the approach temperature.

The Reynolds number is defined as

$$Re = \frac{V_{am} d}{\nu_a} \quad (3)$$

where V_{am} is the velocity of air at the minimum free flow area in the tube bank, and ν_a the kinematic viscosity of air at the approach temperature.

Figure 3 shows the Nusselt number averaged over the sample tubes in the bank. The abscissa shows the Reynolds number. Along with the data shown are the predictions based on the correlation developed by Zukauskas [18] for smooth tube banks, and that by Briggs and Young [19] for finned tube banks. The Zukauskas correlation overpredicts the data of the smooth tube bank by almost 20% and the Briggs-Young correlation is also above the data of the finned tube bank by 20%. Those discrepancies, however, are

deemed relatively small in the face of the fact that the bases of those correlations, such as the tube bank geometry and the method of heat transfer measurements, are different from the present one.

The finned tube data are above the smooth tube data by the factor of 3.5 when compared on the equal Reynolds number basis, while the real surface area on the finned tube is 6.53 times the surface area of the smooth tube. The fin efficiency of the finned tube is estimated at above 0.98, hence, this ratio of heat transfer enhancement, which is lower than the surface area increase, is attributable to the fluid mechanics of flow through the tube bank.

The data of the microfinned tubes fall above the smooth tube data by about 17% at a Reynolds number of 9000. This enhancement of heat transfer is less than that obtained with the single tube [15]. This may be attributed to the difference in the fluid flow pattern across the tube bank from that past a single tube in a wide duct. The slope of the line combining the data points is a little steeper than that of the Zukauskas prediction, showing the characteristics of heat transfer from cylinders having rough surfaces which was discussed regarding the single tube data in ref. [15].

It is concluded that the data in Fig. 3 prove the reasonableness of the present data sampling. The conclusion is based on the agreement of the $Nu-Re$ slopes for the smooth and finned tubes with those of the existing correlations, and also the agreement between the predictions and the experimental data within a reasonably close range.

The inspection of local heat transfer coefficients confirms the characteristics of heat transfer in the tube bank reported in the literature [18]. That is, the local heat transfer coefficient in tube rows is 20–60% higher than that on the first row.

Heat transfer to mist flows

Before the presentation of heat transfer data, a generic exposition regarding the relationship between a heat transfer coefficient and temperature difference is given in order to facilitate the interpretation of the data.

To begin with, the attention is focused on a tube singled out from the tube bank. The tube is wetted by water droplets landing on the surface from the stream as well as by drainage from the tubes on the upper rows. Figure 4 shows three curves representing

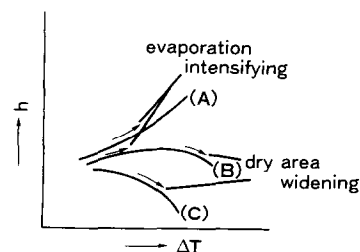


FIG. 4. Physical interpretation of the curves of heat transfer coefficients on mist cooled tube surfaces.

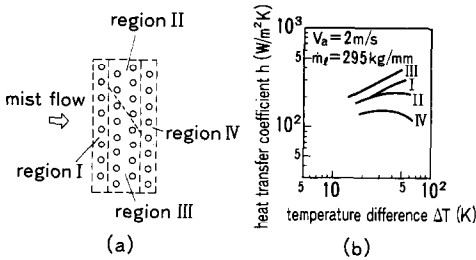


FIG. 5. (a) Division of the tube bank cross-section into subregions, (b) according to the h - ΔT characteristics.

the typical relationships between the heat transfer coefficient and temperature difference. It is assumed that the rate of water supply on the tube, the arrested droplets plus the drainage, is constant for each tube. Curve A shows the case of a sufficiently large rate of water supply. The tube is fully wet, so that as the temperature difference (ΔT) increases, intensifying evaporation raises the heat transfer coefficient. Curve B is the case of a moderate water supply rate. In the range of small ΔT the heat transfer coefficient increases with increasing ΔT due to intensified evaporation. As ΔT increases beyond a certain level, the enlargement of the dry area on the tube's surface takes effect; the heat transfer coefficient levels off, then starts to decline. Curve C is the case of a lean water supply, where the effect of evaporative heat transfer diminishes as ΔT increases.

In the real tube bank placed in the mist stream, the water supply rate on a tube under attention could not be independent of ΔT . As ΔT increases, the rate of evaporation on other tubes changes, hence, the spatial distribution of the local supply rate of water within the tube bank is altered even where the total rate of water supply in front of the bank is kept constant.

The shape of the h - ΔT curve, therefore, reflects not only the effect of evaporation on the tube but also the variation of the water supply rate on that tube with ΔT . Based on the inspection of the data, the cross-section of the tube bank is divided into the subregions as shown in Fig. 5(a). In each subregion the h - ΔT curve bears a characteristic shape; the curves are shown in Fig. 5(b) drawing the example from the data of the smooth tube bank.

Region I contains the tubes on the first row, where the h - ΔT relationship, represented by curve I in Fig. 5(b), is close to that of the single tube.

Region II contains the tubes located in the upper part of the second and third rows. As depicted by curve II in Fig. 5(b) h is at about the same level as on the first row when ΔT is small, however, it tends to level off with increasing ΔT . This characteristic is similar to that of curve B in Fig. 4. This h - ΔT characteristic reflects the state of the water supply to the tubes in region II, namely, the density of water droplets in the flow is reduced behind the first row, and the supply by drainage is also small in the upper part of the tube bank.

The tubes in the lower part of the second and third

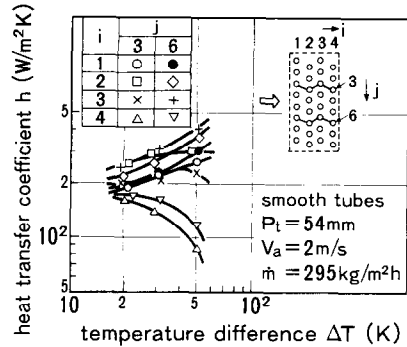


FIG. 6. Heat transfer coefficients on mist cooled smooth tubes.

rows, region III, receive a comparatively ample water supply, mainly the drainage from region II and the upper part of region I. High heat transfer coefficients are obtained here. The heat transfer coefficient increases with increasing ΔT (curve III in Fig. 5(b)) through the mechanism explained for curve A in Fig. 4.

Region IV corresponds to the fourth row of the tube bank, where the supply rate of water is small due to the removal of water droplets by the tubes on the upstream rows and lean supply of drainage. The h - ΔT curve (region IV in Fig. 5(b)) becomes similar to curve C in Fig. 4, reflecting the state of lean water supply.

The regional division in Fig. 5(a) is, of course, based on qualitative characterizations of the h - ΔT relationship. There are no clearly marked boundaries separating the regions, particularly between regions II and III. Nevertheless, with the understanding about this qualitative nature of the zoning, the notion of the regional area is introduced for regions II and III. Region II borders region III at the slant boundary as depicted in Fig. 5(a). This boundary advances downward when ΔT is increased. The same effect is achieved by the reduction of the rate of water injection into the main stream. The representative h - ΔT relationships in the subregions are also affected by the air velocity, the mist density, the tube geometry, and the tube pitch. In what follows, the effects of those parameters on heat transfer are shown drawing examples from the body of data.

Figure 6 shows the data obtained with the smooth tube bank at the air velocity of 2 m s^{-1} and the water mass flux of $295 \text{ kg m}^{-2} \text{ h}^{-1}$. The location of the tube is indicated by the index (i, j), where i is the number attached to the vertical row and j is the number for the horizontal row. The identification of data symbols is given by the inset in the figure. The figure is just the detailed reproduction of Fig. 5(b). When compared with the performance of the tube bank in single phase flows in terms of the averaged heat transfer coefficient at equal air velocity, mist cooling enhances heat transfer by a factor of 3–5. The effect of air velocity on the heat transfer coefficient is less pronounced in

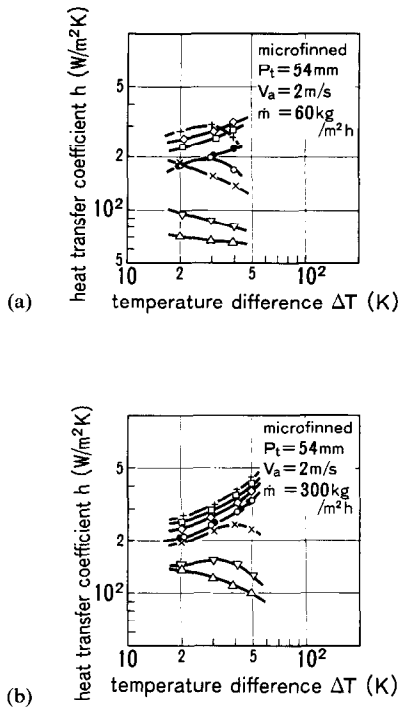


FIG. 7. Heat transfer coefficients on mist cooled microfinned tubes (for the identification of data symbols, see the inset in Fig. 6): (a) water mass flux $\dot{m} = 60 \text{ kg m}^{-2} \text{ h}^{-1}$; (b) water mass flux $\dot{m} = 300 \text{ kg m}^{-2} \text{ h}^{-1}$.

mist flows than in single phase flows; the heat transfer coefficient in the case of mist flows is proportional to $V_a^{0.4}$ while in the case of single phase flows to $V_a^{0.6}$. For the interpretation of this finding the heat transfer mechanisms on the wet and dry areas of the tube's surface and the ratio of wet area to dry area need be considered. The approximate analysis of the heat transfer process is developed in the next section.

The effect of mass flux of water on heat transfer is shown for the case of a microfinned tube bank in Fig. 7. The air velocity is 2 m s^{-1} , the mass flux of water for the data in Fig. 7(a) is $60 \text{ kg m}^{-2} \text{ h}^{-1}$, and that for Fig. 7(b) is $300 \text{ kg m}^{-2} \text{ h}^{-1}$. The inset of Fig. 6 gives the correspondence between the data symbols and the tube locations. The increase in water supply is particularly effective in raising the heat transfer coefficient in region IV and also in regions II and III at large ΔT . The data in Figs. 6 and 7(b) were obtained at the almost equal rate of water flux. The comparison of these data indicates that the effectiveness of microfins becomes pronounced with increasing ΔT , especially on the tubes in the upper part of the first and second rows. Enhancement of heat transfer is also observed for the other sampled tubes, though on some of them it is of an invisible magnitude in the graph. The increased effectiveness of microfins at large ΔT is a characteristic common to the data of the single tube [15]. The analysis of the data developed for the single tube [15] implies that this effectiveness is produced by the increased role of evaporation in heat transfer at

large ΔT and the extension of the wet area on the finned surface by capillary action. The relative merit of water injection as compared to the performance in single phase flows is of the same order of magnitude with that obtained for the smooth tube bank; that is, a factor of 4–5 in terms of the average heat transfer coefficient.

The effect of the tube pitch on heat transfer was investigated using the microfinned tube bank. Comparison was made of the data obtained with the tube pitch of 54 mm and those of 42 mm at equal frontal air velocity and water mass flux. It was found that the closer tube arrangement reduces the heat transfer coefficient on the tubes in the upper part of the third row; the reduction is particularly significant at large ΔT . Low heat transfer coefficients were also observed for the tubes in the fourth row. In other words, region II defined in Fig. 5(a) contains a larger number of tubes, and the deterioration of heat transfer in region IV becomes significant in a closely packed tube bank. This is an indication of the lower effectiveness of mist cooling on the tubes in the downstream rows due possibly to the increased removal of water droplets on the first row.

Figure 8 shows the data obtained with the bank of finned tubes at an air velocity of 2 m s^{-1} and a water mass flux of $220 \text{ kg m}^{-2} \text{ h}^{-1}$. The tube pitch is 42 mm. This small tube pitch and the presence of 5 mm high fins make the free flow area in the tube bank markedly smaller than those in the smooth and microfinned tube banks. This narrowness of the free flow area and the large surface area on the finned tubes increase the

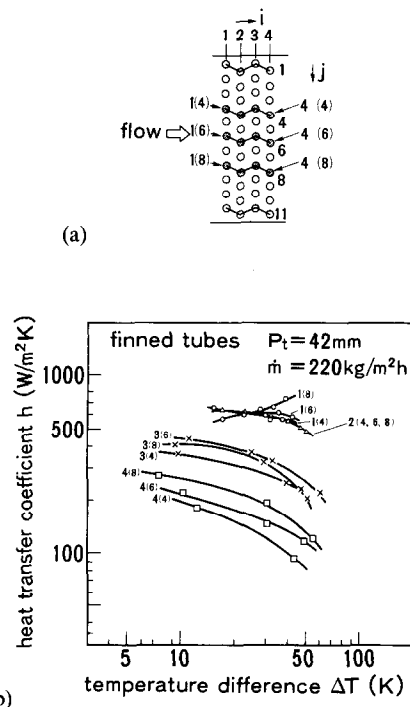


FIG. 8. Heat transfer coefficients on mist cooled finned tubes: (a) sampled tube locations; (b) $h-\Delta T$ at $V_a = 2 \text{ m s}^{-1}$.

efficiency of arresting water drops, thereby produce the state of relatively lean water supply on most of the tubes, as exhibited by the data shown in Fig. 8. Figure 8(a) shows the locations of the sampled tubes and the identification indices. The first figure indicates the number attached to the vertical row, i , and the figure in parentheses the number attached to the horizontal row, j . Among the curves in Fig. 8(b) only that for the number 1(8) has the characteristic of curve A of Fig. 4. On the other tubes the increase in ΔT causes a decrease in h .

There are some more points worthy of attention in the data obtained with the finned tube bank.

The high heat transfer coefficients on the first and second vertical rows contribute to the high performance of the finned tube bank.

Heat transfer coefficients of the finned tubes are higher than those of the smooth tubes, however, the effect of fins in mist flows is not so pronounced as that in single phase flows. This observation is based on comparison of the single phase flow data in Fig. 3 and the mist flow data in Figs. 8(b) and 6. The reduced merit of providing fins in the case of mist cooling, particularly on the tubes in the downstream rows and at large ΔT , is attributable more to the enhanced heat transfer on mist cooled smooth tubes than to the ineffectiveness of the fins.

The microgrooving of the fin surface yields a certain effect on heat transfer. Compared to the performance of the tube equipped with smooth fins of the same dimension, the present finned tube yields 20–40% higher heat transfer coefficients at a given set of mist flow parameters. The relative merit of microgrooves is higher at large water supply rates and large ΔT .

ANALYSIS OF DATA OF MIST COOLED TUBE BANKS

As exhibited by the example data in Figs. 6–8, the heat transfer coefficient in the mist cooled tube banks depends to a considerable extent on ΔT . The relationship between h and ΔT varies through a complex function of the tube geometry, the tube pitch, the air velocity, and the water mass flux. A conclusion derived from the study of the data is that evaporation of water on wetted surface areas is a primary mechanism of heat transfer enhancement.

In this section the empirical formulas are derived, which correlate the wet surface area to the enthalpy potential for evaporation, the water supply rate, and the air velocity. Such a correlation is indispensable in the design of mist cooled heat exchangers.

The analysis of the data is based on the physical model and the assumptions summarized as follows.

(1) The flow and thermal fields are uniform in the plane perpendicular to the main stream. Hence, the density of water droplets riding in the stream and the air temperature vary in the streamwise direction alone. The water mass flux is denoted by $\dot{m}_{(i)}$, and the dry

bulb temperature of air by $T_{a(i)}$, where i is the index attached to the vertical tube column.

(2) The rate of arrest of water droplets on the tube's surface is equal to the mass flux $\dot{m}_{(i)}$ times the frontal area of the tube, that is the area perpendicular to the stream, A_c . The mass flux at the downstream row ($\dot{m}_{(i)}, i > 1$) is determined from the mass balance consideration. Namely, the sum of water mass arrested by the upstream rows per unit time is subtracted from the supply rate of water at the front of the tube bank, and the resultant difference is divided by the cross-sectional area of the tube bank.

(3) The rate of water supply at the tube (i, j) , $\dot{m}_{(i,j)}$, is given by

$$\dot{m}_{(i,j)} = \dot{m}_{(i)} + \dot{M}_{d(i,j-1)}/A_c \quad (4)$$

where $\dot{M}_{d(i,j-1)}$ is the rate of water drainage from the tubes above.

(4) The temperature of water droplets riding in the stream is assumed to be equal to the wet bulb temperature measured at the front of the tube bank, T_{as} .

(5) The temperature is almost uniform over the surface area of the tube. Even on the finned tube this assumption holds with good accuracy, for the fin efficiency in this experiment is about 0.98 at minimum.

(6) The difference between the tube temperature and the temperature of the water film on the tube's surface is negligibly small. Both temperatures are denoted by the same symbol T_w .

(7) The rate of enthalpy transfer by the drainage of water from the tube is negligibly small compared to the other modes of heat transfer on the tube. However, the rate of drainage is important for the estimation of water supply on the tube under attention, through equation (4).

(8) The convective heat transfer coefficient, $h_{c(i)}$, on the dry area as well as on the surface of the water film is given by the data of single phase flow experiments. The data of single phase flow experiments are correlated by the following equations, where Nusselt number is defined on the basis of the difference between the tube wall temperature and the mixed mean temperature of air at row i , $Nu_{c(i)} \equiv h_{c(i)}d/k_a$.

For the smooth tubes

$$Nu_{c(i)} = 0.20\phi_{(i)} Re^{0.6} \quad (5)$$

where $\phi_{(i)}$ is the coefficient attached to row i

$$\phi_{(1)} = 1.0, \quad \phi_{(2)} = 1.2, \quad \phi_{(3)} = 1.6, \quad \phi_{(4)} = 1.5.$$

For the microfinned tubes

$$Nu_{c(i)} = 0.13\phi_{(i)} Re^{0.66} \quad (6)$$

$$\phi_{(1)} = 1.0, \quad \phi_{(2)} = 1.5, \quad \phi_{(3)} = 1.6, \quad \phi_{(4)} = 1.4.$$

For the finned tubes

$$Nu_{c(i)} = 0.66\phi_{(i)} Re^{0.6} \quad (7)$$

$$\phi_{(1)} = 1.0, \quad \phi_{(2)} = 1.5, \quad \phi_{(3)} = 1.5, \quad \phi_{(4)} = 1.4.$$

The above correlations are based on the data in

the range of Reynolds numbers of 3×10^3 – 1.2×10^4 .

(9) The evaporation from the surface of the water film is governed by the Lewis law, where the driving potential for evaporation is the difference between the absolute humidity of saturated air at the tube temperature, $x_{1(i,j)}$, and that in the air stream, $x_{(i)}$. The latter is estimated from the humidity at the front of the tube bank and the sum of evaporated water on the upstream rows.

Based on the above modeling the rate of evaporation from the tube (i, j) and the part of the surface area effective for evaporation $A_{ev(i,j)}$ are determined from the following equations.

Convective heat transfer

$$Q_{c(i,j)} = h_{c(i)}(T_w - T_{a(i)})A \quad (8)$$

where A is the heat transfer area of the tube.

Enthalpy input to the tube (i, j) from the arrested water droplets

$$Q_{s(i,j)} = \dot{m}_{(i)} A_c c_{pl}(T_w - T_{as}) \quad (9)$$

where c_{pl} is the heat capacity of water.

Heat balance on the tube (i, j)

$$Q_{(i,j)} = Q_{L(i,j)} + Q_{c(i,j)} + Q_{s(i,j)} \quad (10)$$

where $Q_{(i,j)}$ is the measured heat transfer rate, and $Q_{L(i,j)}$ is the transfer rate of latent heat by evaporation of water.

Once the latent heat transport is found, the evaporation rate of water on the tube (i, j) is determined from

$$\dot{M}_{ev(i,j)} = \frac{Q_{L(i,j)}}{h_{fg}} \quad (11)$$

where h_{fg} is the latent heat of evaporation.

The effective area for evaporation is then computed from

$$A_{ev(i,j)} = \frac{c_{pa} \dot{M}_{ev(i,j)}}{h_{c(i)}(x_{1(i,j)} - x_{(i)})} \quad (12)$$

where c_{pa} is the specific heat of air.

From the mass balance of water on the tube (i, j) , the rate of drainage leaving the tube is determined as

$$\dot{M}_{d(i,j)} = \dot{m}_{(i)} A_c - \dot{M}_{ev(i,j)} + \dot{M}_{d(i,j-1)} \quad (13)$$

The computation is started from the tube $(1, 1)$, where $\dot{M}_{d(1,0)} = 0$, then first advanced downward along the first vertical row $(1, j)$. The drainage from a tube was assumed to strike the tube immediately below. This assumption is admittedly crude; nevertheless, this is considered the only practical way of performing the data reduction. The air temperature $T_{a(2)}$ approaching the second row is raised from the air temperature in front of the first row by

$$\sum_j Q_{c(1,j)} / c_{pa} \dot{M}_a$$

where the summation is made over the entire column, and \dot{M}_a is the mass flow rate of air.

The absolute humidity of air near the second row

is computed by adding the mass of evaporated water on the first row to the initial humidity. Once the streaming flux of water droplets and the humidity are determined, the computation proceeds from the tube $(2, 1)$ downward, finding $A_{ev(2,j)}$ and $\dot{M}_{d(2,j)}$ through equations (4)–(13). The computation is repeated for the third and fourth rows.

Figures 9(a)–(c) show the ratio of the effective wet area to the heat transfer area of the tube; (a) for the smooth tube, (b) for the microfinned tube, and (c) for the finned tube. The abscissa shows the rate of water supply per unit frontal area of the tube, \dot{m}_t . In Figs. 9(a) and (b), the air velocity is 2 m s^{-1} . The two sets of data are plotted; the one for the case of $\Delta T = 20 \text{ K}$, and the other for $\Delta T = 40 \text{ K}$.

Plotted in Fig. 9(c) are the data for the combinations of air velocity and temperature difference; 1 and 2 m s^{-1} , 25 and 35 K. Also shown are the data obtained with another experimental apparatus where large rates of water supply were given from the supply tube located above the test tube.

There are basically three modes of contribution from the wet area to heat transfer; each mode exists in a certain range of \dot{m}_t . In Figs. 9(a) and (b) the ranges of these modes are indicated for the case of $\Delta T = 20 \text{ K}$ and in Fig. 9(c) for $\Delta T = 25 \text{ K}$.

In mode I the water supply is relatively lean, so that the effective wet area increases as the water supply increases. In mode II a large part of the tube's surface area is covered by a water film, and the wet area no longer expands with increasing \dot{m}_t . As the water supply exceeds a certain value, the water film on the surface becomes excessively thick, posing an increased thermal resistance. In this range of mode III, although the tube surface is nearly flooded by water, the effectiveness of the wet area, that is represented here by the effective area for evaporation, decreases with increasing \dot{m}_t .

The following correlations are derived from the data obtained by the present experiments. Suffixes (i) , (j) , and (i, j) attached to the symbols in equations (4)–(13) are omitted here for the sake of simplicity.

The smooth tube; in mode I

$$\frac{A_{ev}}{A} = \frac{\dot{m}_t A_c c_{pa}}{h_c(x_1 - x)A} \quad \text{for } A_{ev}/A < 0.5 \quad (14)$$

$$\frac{A_{ev}}{A} = 30.1 \Delta i^{-0.37} \dot{m}_t^{0.30} V_{am}^{-0.40}$$

$$\text{for } 0.5 < A_{ev}/A < 0.9 \quad (15)$$

where Δi is the enthalpy difference between the saturated air at the tube wall temperature and the air in the stream, and

$$\frac{A_{ev}}{A} = 0.9 \quad \text{in mode II.} \quad (16)$$

The microfinned tube; equation (14) holds in mode I ($A_{ev}/A < 0.75$)

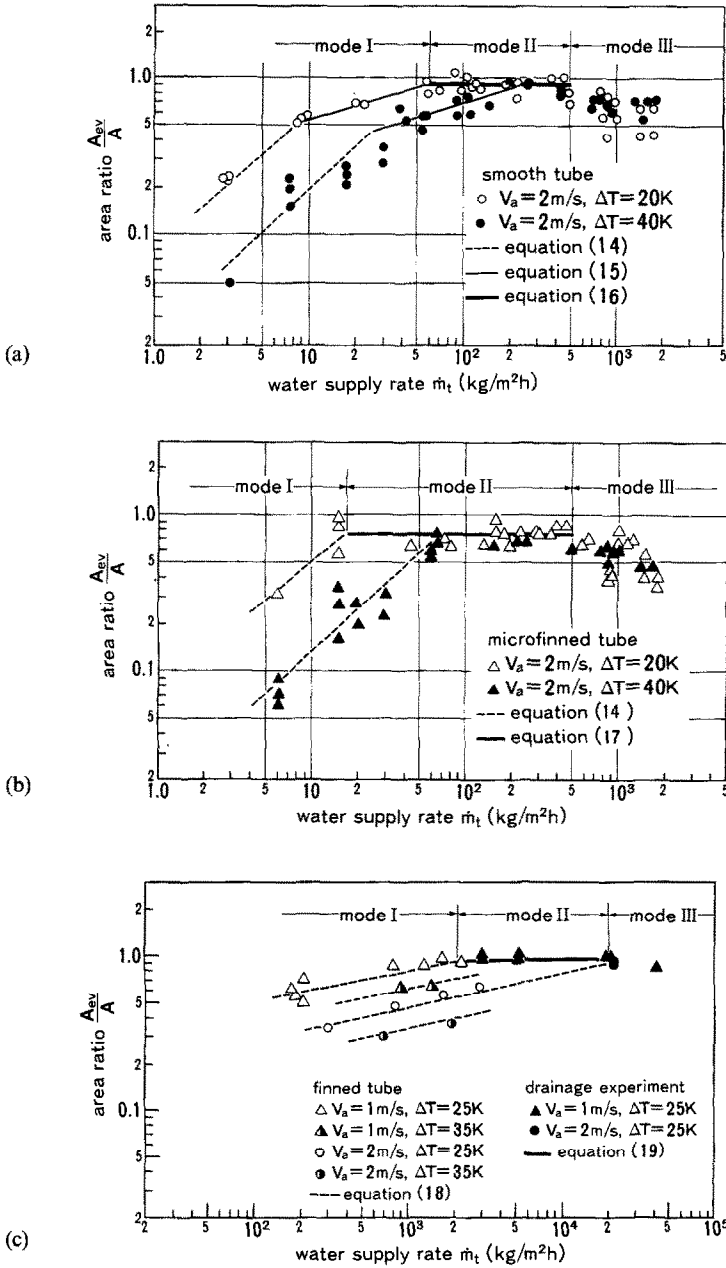


FIG. 9. Relationship between A_{ev}/A and \dot{m}_t : (a) smooth tube; (b) microfinned tube; (c) finned tube.

$$\frac{A_{ev}}{A} = 0.75 \quad \text{in mode II.} \quad (17)$$

The finned tube; in mode I

$$\frac{A_{ev}}{A} = 50.8 \Delta i^{-0.4} \dot{m}_t^{0.20} V_{am}^{0.84} \quad \text{for } A_{ev}/A < 0.9 \quad (18)$$

$$\frac{A_{ev}}{A} = 0.9 \quad \text{in mode II.} \quad (19)$$

On all the tubes tested in this investigation mode III appears when the specific water supply rate \dot{m}_t

exceeds $500 \text{ kg m}^{-2} \text{ h}^{-1}$. It is found that the correlation developed for conventional wet towers [20], where the tubes are flooded by circulating water, also works well to correlate the present data.

Equations (14)–(19) are represented by broken and solid lines in Fig. 9. These correlations obtained by the laboratory experiments are used in the design analysis of full-scale heat exchangers. The steps of mist cooled heat exchanger design are essentially the retracing of the data reduction explained above. After the input of data, which specifies the tube wall temperature, the air flow rate, and the mass flux of water in front of the tube bank, the water supply rate on the

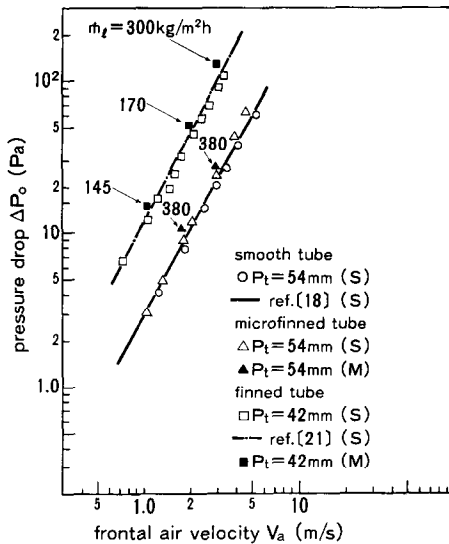


FIG. 10. Pressure drop across the tube bank.

tube, $\dot{m}_{(i,j)}A_{c,i}$, is computed from equation (4). The effective area for evaporation is then computed from the correlations developed above. Equation (12), after rearrangement of the terms, is used to find the evaporation rate from the tube (i, j) , $\dot{M}_{ev(i,j)}$, which then gives the latent heat transport through equation (11). After computing the contributions from convective heat transfer (equation (8)) and enthalpy of arrested water droplets (equation (9)), the heat transfer rate is determined from equation (10). The rate of drainage from the tube (i, j) is computed from equation (13), which in turn is used to find the water supply rate on the tube $(i, j+1)$.

This method of performance analysis was tested in the design of mist cooled condensers, and the accuracy was proved by comparison of the prediction and the test data obtained with the prototype condenser [16].

PRESSURE DROP DATA

Figure 10 shows the pressure drop data in single phase flows (S) and mist flows (M) across the tube bank. The abscissa shows the frontal air velocity. The data of the smooth tube bank are compared with the existing correlation cited in ref. [18], and the data of the finned tube bank are compared with the Jameson correlation [21]. Good agreement is found between the single phase flow data and those predictions. Moreover, it is found that the difference between the pressure drop in mist flows and that in single phase air flows is very small. This suggests that, with a given fan power, enhancement of heat transfer of 300–500% could be obtained by injecting water into the stream without the penalty of reduced air velocity.

CONCLUSIONS

Fine water droplets were injected into the air stream, and their effect on the heat transfer per-

formance of the cross flow tube banks was investigated. The attention was focused on the cases of low air velocities ($1\text{--}3\text{ m s}^{-1}$) and relatively small rates of water injection ($50\text{--}390\text{ kg m}^{-2}\text{ h}^{-1}$). The following conclusions are obtained.

(1) Averaged heat transfer coefficients of the tube bank could be raised markedly by the water injection without penalty of increased flow resistance. The present experimental data show 300–500% of heat transfer enhancement.

(2) The heat transfer coefficient on individual tubes depends to a considerable extent on the temperature potential ΔT . This suggests the importance of evaporation of water from the wetted part of the tube's surface in enhancement of heat transfer. Further corroborations of the importance of evaporation are given by the observed effectiveness of microstructures provided on the heat transfer surface.

(3) Water is supplied to the tube through the two routes, the arrest of streaming water droplets on the heat transfer surface and the reception of dripping water from the tubes on upper rows. The extent of surface wetting and its effectiveness in heat transfer enhancement are different on the tubes having different surface geometries. Tested were the smooth tubes, the microfinned tubes, and the finned tubes. Their heat transfer data are interpreted in the light of the physical models which produce characteristic $h\text{--}\Delta T$ relationships.

(4) The empirical formulas are derived, which correlate the effective wet area on the tube's surface to the operative parameters such as the water supply rate, the enthalpy potential for evaporation, and the air velocity. The method of design analysis based on these correlations is proposed.

Acknowledgement—This work was initiated in a part of the program "Development of Binary Cycle Power Plants Based on the Energy of Geothermal Brine", promoted and sponsored by the Ministry of International Trade and Industry, and the New Energy Development Organization, Japan, since 1979. Professor Y. Mori has been serving as chairman of the executive committee of this program. The authors note their deep appreciation toward Professor Mori for his leadership in execution of the research program.

REFERENCES

1. Y. Mori and W. Nakayama, High performance mist cooled condensers for geothermal binary cycle plants. In *Heat Transfer in Energy Problems* (Edited by T. Mizushima and W. J. Yang), pp. 189–196. Hemisphere, Washington, DC (1982).
2. B. M. Johnson, F. R. Zaloudek, H. D. Fricke, R. G. Helenbrook and J. A. Bartz, A large-scale experimental evaluation of an advanced concept for dry/wet cooling of power stations, U.S./U.S.S.R. Symposium on Waste Heat, Washington, DC (Oct. 1979).
3. W. Leidenfrost and B. Korenic, Analysis of evaporative cooling and enhancement of condenser efficiency and of coefficient of performance, *Wärme- und Stoffübertr.* **12**, 5–23 (1979).
4. I. C. Finlay and T. McMillan, Pressure drop, heat and mass transfer during air/water mist flow across a bank of

- tubes, National Engineering Laboratory, NEL-Report No. 474 (1970).
5. T. Oshima, S. Iuchi, A. Yoshida and K. Takamatsu, Design calculation method of air-cooled heat exchangers with water spray, *Heat Transfer—Jap. Res.* **1**, 47–55 (1972).
 6. D. R. Tree, V. W. Goldshmit, R. W. Garrett and E. Kach, Effect of water sprays on heat transfer of a fin and tube heat exchanger, *Proc. 6th International Heat Transfer Conference*, **HX-26**, 339–344 (1978).
 7. R. A. Carpenter, Heat transfer coefficients for two-phase (water/air) flow over a tube bank, United States Air Force, Report No. GNE/PH/72-2 (May 1972).
 8. H. C. Simpson, G. C. Beggs and G. N. Sen, Heat transfer from extended surface tubes to an air/water mist, *Proceedings of the Symposium on Multiphase Flow Systems*, Inst. Chem. Engrs Ser., No. 38, Paper No. H3, pp. 1–22 (1974).
 9. I. C. Finlay, Air/water sprays as potential coolants for pin-finned cold plates, Aerospace Research Laboratories ARL71-0087 (1971).
 10. W. J. Yang and D. W. Clark, Spray cooling of air-cooled compact heat exchangers, *Int. J. Heat Mass Transfer* **18**, 311–317 (1975).
 11. T. Aihara and R. Saga, Performance of a cooling unit with a mist generating blower, *Trans. Japan Soc. Mech. Engrs*, Ser. B **49**, 2410–2417 (1983).
 12. D. Pescod, A heat exchanger for energy saving in an air-conditioning plant, *Trans. ASHRAE* **85**, 238–251 (1979).
 13. Y. Hayashi and A. Takimoto, Heat transfer enhancement with mist flow. In *Heat Transfer in High Technology and Power Engineering* (Edited by W. J. Yang and Y. Mori), pp. 356–367. Hemisphere, New York (1987).
 14. I. L. Maclaine-Cross and P. J. Banks, A general theory of wet surface heat exchangers and its application to regenerative evaporative cooling, *Trans. ASME*, Ser. C **103**, 579–585 (1981).
 15. H. Kuwahara, W. Nakayama and Y. Mori, Heat transfer from the heated cylinders with various surfaces in air/water mist flows, *Heat Transfer—Jap. Res.* **10**, 1–19 (1981).
 16. S. Hirasawa, H. Kuwahara, W. Nakayama and Y. Mori, Optimization of mist cooled condensers for geothermal binary cycle plants, *Proceedings ASME/JSME Thermal Engineering Joint Conf.* **2**, 133–138 (1983).
 17. K. Fujie, W. Nakayama, H. Kuwahara, Y. Nakayama and K. Kakizaki, High-flux heat transfer tubes “THERMOEXCEL’s”: their performance and the results of feasibility test in a refrigerating machine, *Proc. XIV International Congress of Refrigeration*, Vol. II, pp. 633–638 (1975).
 18. A. Zukauskas, Heat transfer from tubes in cross flow. In *Advances in Heat Transfer* (Edited by J. P. Hartnett and T. F. Irvine, Jr.), pp. 93–160. Academic Press, New York (1972).
 19. D. E. Briggs and E. H. Young, Convection heat transfer and pressure drop of air flowing across triangular pitch banks of finned tubes, *Chem. Engng Prog. Symp.* **59**, 1–10 (1965).
 20. T. Mizushina, A. Itoh and O. Miyashita, Performance of evaporative coolers and the method of design analysis, *Kagaku Kogaku (Chem. Engng)* **32**, 55–61 (1968).
 21. S. L. Jameson, Tube spacing in finned tube banks, *Trans. ASME* **67**, 633–642 (1945).

TRANSFERT THERMIQUE POUR UN BANC DE TUBES ET UN ECOULEMENT D'AIR AVEC BROUILLARD D'EAU

Résumé—On mesure le transfert de chaleur et la perte de pression sur des bancs de tubes lisses, de tubes micro-ailetés, et de tubes ailetés placés dans un écoulement de brouillard, pour une vitesse d'air entre 1 et 3 m s⁻¹, et un flux-masse d'eau entre 50 et 390 kg m⁻² h⁻¹. Des examens croisés des données de transfert de chaleur montrent que l'évaporation d'eau sur la surface mouillée est un mécanisme premier de l'augmentation du transfert de chaleur. A partir des formules empiriques de l'aire effectivement mouillée sur la surface de transfert, la méthode est proposée pour la conception de l'échangeur de chaleur. Les données de perte de pression montrent une petite différence entre celle pour l'écoulement de brouillard et celle pour l'écoulement d'air seul.

DER WÄRMEÜBERGANG AN ROHRBÜNDELN IN EINER LUFT/WASSER-NEBELSTRÖMUNG

Zusammenfassung—An Bündeln aus glatten, feinstberippten und berippten Rohren in einer Nebelströmung wurden Wärmeübergang und Druckabfall bei einer Luftgeschwindigkeit von 1–3 m s⁻¹ und bei einer Massenstromdichte des Wassers von 50–390 kg m⁻² h⁻¹ ermittelt. Es zeigte sich, daß die Verdunstung von Wasser an benetzten Teilen der Oberfläche in erster Linie für die Erhöhung des Wärmeübergangs verantwortlich ist. Basierend auf den empirischen Korrelationen für die wirksame benetzte Zone der wärmeübertragenden Oberfläche wird ein Verfahren für die Wärmetauscher-Auslegung vorgeschlagen. Beim Druckabfall zeigte sich kaum ein Unterschied zwischen dem Strömungswiderstand in Nebelströmungen und dem in einphasigen Luftströmungen.

ТЕПЛОБМЕН ПАКЕТА ТРУБ В ПОТОКЕ АЭРОЗОЛИ ВОЗДУХ/ВОДА

Аннотация—Получены данные по теплообмену и перепаду давления для пакетов гладких труб, труб с микрооребрением и оребранных труб, помещенных в поток аэрозоли, в котором скорость воздуха и массовый поток жидкости составляли, соответственно, 1–3 м/с и 50–390 кг/м²ч. Рассмотрение данных по теплообмену показывает, что испарение воды с увлажненной части поверхности является первичным механизмом, усиливающим теплообмен. Предложен метод проектирования теплообменников, основывающийся на эмпирических зависимостях для зоны эффективного смачивания на поверхности теплообмена. Данные по перепаду давления показывают малое отличие сопротивлений в потоках тумана и однофазных потоках воздуха.